chemosensors

MDPI

Article

Tetracycline Antibiotics: Elucidating the Electrochemical Fingerprint and Oxidation Pathway

Rocío Cánovas [1,2], Nick Sleegers [1,2], Alexander L.N. van Nuijs [3] and Karolien De Wael [1,2,*]

1 AXES Research Group, Bioscience Engineering Department, University of Antwerp, Groenenborgerlaan 171, 2020 Antwerp, Belgium; rocio.canovasmartinez@uantwerpen.be (R.C.); nick.sleegers@uantwerpen.be (N.S.)
2 NANOlab Center of Excellence, University of Antwerp, Groenenborgerlaan 171, 2020 Antwerp, Belgium
3 Toxicological Center, University of Antwerp, Universiteitsplein 1, 2610 Antwerp, Belgium; alexander.vannuijs@uantwerpen.be
* Correspondence: karolien.dewael@uantwerpen.be

Abstract: Herein, a complete study of the electrochemical behavior of the most commonly used tetracycline antibiotics (TCs) on unmodified carbon screen-printed electrodes (SPEs) is presented. In addition, the oxidation pathway of TCs on SPE is elucidated, for the first time, with liquid chromatography-quadrupole time-of-flight mass spectrometry (LC-QTOF-MS). Square wave voltammetry (SWV) was used to study the electrochemical fingerprint (EF) of the antibiotics shaping the different oxidation processes of the TCs in a pH range from 2 to 12. Their characteristic structure and subsequent EF offer the possibility of distinguishing this class of antibiotics from other types. Under the optimized parameters, calibration curves of tetracycline (TET), doxycycline (DOXY), oxytetracycline (OXY), and chlortetracycline (CHL) in a Britton Robinson buffer solution (pH 9) exhibited a linear range between 5 and 100 µM with excellent reproducibilities (RSD_{TET} = 3.01%, RSD_{DOXY} = 3.29%, RSD_{OXY} = 9.78% and RSD_{CHL} = 6.88% at 10 µM, N = 3) and limits of detection (LOD) of LOD_{TET} = 4.15 µM, LOD_{DOXY} = 2.14 µM, LOD_{OXY} = 3.07 µM and LOD_{CHL} = 4.15 µM. Furthermore, binary, tertiary, and complex mixtures of all TCs were analyzed with SWV to investigate the corresponding EF. A dual pH screening (pH 4 and pH 9), together with the use of a custom-made Matlab script for data treatment, allowed for the successful confirmation of a single presence of TCs in the unknown samples. Overall, this work presents a straightforward study of the electrochemical behavior of TCs in SPE, allowing for the future on-site identification of residues of tetracycline antibiotics in real samples.

Keywords: tetracycline antibiotics; electrochemical fingerprint; liquid chromatography mass spectrometry; oxidation pathway

Citation: Cánovas, R.; Sleegers, N.; van Nuijs, A.L.N.; De Wael, K. Tetracycline Antibiotics: Elucidating the Electrochemical Fingerprint and Oxidation Pathway. *Chemosensors* **2021**, *9*, 187. https://doi.org/10.3390/chemosensors9070187

Academic Editors: Manel del Valle, Vahid Hamedpour and Andreas Richter

Received: 4 June 2021
Accepted: 19 July 2021
Published: 20 July 2021

1. Introduction

Tetracycline antibiotics (TCs) produced by *Streptomyces* are broad-spectrum agents characterized by containing four condensed aromatic rings known as naphthacene cores (see Figure S1). TCs are especially effective against a broad variety of Gram-positive and Gram-negative bacteria, such as *Staphylococcus*, *Streptococcus*, *Pneumococcus*, *Gonococcus*, *Cholera*, *Dysentery bacillis*, *Pertussis*, *Rickettsia*, *Chlamydia*, and *Mycoplasma* [1,2]. Since their first introduction into medicine in the 1940s, antibiotics have been widely used in livestock farming—as veterinary medicines, feed additives, growth promoters [3], or to prevent/treat mastitis and metritis in cows [4]—and in healthcare for the treatment of many different infections, such as respiratory tract infections, urethritis and severe acne, or even malaria [5,6]. TCs can be divided into four main types: tetracycline (TET), doxycycline (DOXY), oxytetracycline (OXY), and chlortetracycline (CHL), which are most often applied to livestock animals (including honeybees) because of their affordability [5]. However, during the last decades, the generation of new TCs has increased considerably, with more than nine different types of TC [1]. The action mechanism of TC lies in its active transport

into the cells of the susceptible bacteria, for the inhibition of protein biosynthesis after binding to the 30S ribosomal subparticle [1,7].

In spite of its unquestionably antibacterial clinical application, the excessive use of TCs exhibits important disadvantages and concerns in our society. First, some examples are the possible allergic sensibilization of exposed individuals (raising intracranial pressure and skin infections, such as rosacea or perioral dermatitis) [8] and adverse effects, including gastrointestinal disturbances (due to the selective pressure that antimicrobial drug residues may exert over human gut microflora) and renal dysfunction [6,9]. Moreover, TCs have been described as hepatotoxic, more dangerous during pregnancy [8,10], and carcinogenic agents, therefore, exposure to them should be reduced to the minimum possible level [11]. Finally, the overuse of these antibiotics promotes resistance genes in bacteria [12]. These resistant bacteria may spread from animals to humans via the food chain [13]. Thus, pathogens could possibly become resistant to these drugs leading to a failure risk of the antibiotic treatment, decreasing its efficiency and triggering potential negative effects for both human and animal health [5,13,14].

According to the World Health Organization (WHO), more than half of the global production of antibiotics is used in farm animals [15]. As TCs have been widely used for animal feed, meat, milk, and fish production, the analytical methods developed are mainly focused on their determination in food samples. Although a maximum residue limit (MRL) has been set for these compounds in food-safety control programs in many countries (see Table S1, MRLs established by European Union), a fast and sensitive analytical method is still needed for achieving the lowest possible detection limit [5].

On the other hand, as TCs are difficult to completely decompose in the body of animals and people, significant quantities of the toxic TC are discharged into the environment [16]. In this way, residues of TCs can also be heavily adsorbed into environmental materials, as well as in waste effluents from hospitals and pharmaceutical industry, where they keep their activity, leading to bacterial resistance [17]. For example, it has been demonstrated that OXY remains undegraded for more than ten months when it is adsorbed in marine sediments and soils [17]. A few studies have reported that the concentration of TCs in groundwater and surface water is as high as 0.2–10 nM, which may be sufficient to cause serious pollution of the aquatic environment [16]. However, the possible contamination of ground water is largely unknown [18], and the exhaustive control of these residues in the environment should be addressed in the near future [19,20]. Hence, accurate monitoring, based on highly sensitive and selective user-friendly sensors for in situ application, is urgently required.

Electrochemical-based detection is of particular interest due to its remarkable advantages, such as low cost, excellent sensitivity, portability, and fast response in comparison to laboratory-based equipment such as high-performance liquid chromatographic (HPLC), spectrophotometry, or capillary electrophoresis, which require relatively expensive instrumentation, have long analysis times, and entail trained personnel [6,21]. Moreover, electrochemical sensors manufactured using screen-printing technology offer huge advantages, utilizing the progressive drive towards miniaturized, sensitive, and portable device and making them user-friendly and disposable [22].

During the last decades, the electrochemical detection of several types of TCs has been pursued using different approaches. Biorecognition is one of the most common strategies and uses aptamer-based sensors [23–32], which are the most recent and commonly found in the literature, followed by enzyme-linked immunoassay (ELISA) functionalization [14,15,33,34], and sensors based on molecular imprinted polymers (MIPs) [35,36] or antibodies [8,37,38] (see Table S2). Furthermore, the oxidation of TCs has been reported using diverse types of electrodes and materials, ranging from metallic nanoparticles [39–45], graphene oxide [46–50], composites [43,51–55], gold [3,11,56], boron-doped diamond electrode (BDDE) [57–60], ruthenium oxide-hexacyanor-uthenate (RuO-RuCN) [61], or multiwall carbon nanotubes (MWNTs) [17,21] (Table S3). Interestingly, several cases have shown a combination of electrochemical detection (ED) with other analytical methods, such as

HPLC [59,62,63], as well as flow-injection (FI) [6,57,58,64–66] (see Table S3). However, to date, few studies have explored and reported an understanding of the basis of the electrochemistry of TCs per se. One example is the work reported by Hou et al., where the authors studied the electrochemical behavior of four different TCs by cyclic voltammetry and differential pulse voltammetry at electrochemically pre-treated glassy carbon electrodes [67]. Furthermore, there is a lack of information and publications specifically showing the oxidation pathways and their corresponding oxidation products.

Herein, a meaningful study of the electrochemical behavior of the most commonly used TCs (TET, DOXY, OXY, and CHL) on carbon screen-printed electrodes (SPE), as well as the elucidation of the oxidation pathway on the SPE via liquid chromatography-quadrupole time-of-flight mass spectrometry (LC-QTOF-MS), is for the first time presented. First, the voltammetric response of the four TCs at different pHs (ranging from 2 to 12) was measured, to explore their characteristic electrochemical fingerprints (EF). Afterwards, the selective identification of single TCs and the influence of binary and complex mixtures on the EF of TCs was studied by square wave voltammetry (SWV), using a dual pH strategy (pH 4 and pH 9). Moreover, a custom-made data treatment based on Matlab software was used to enhance the peak separation, thus facilitating the identification of the TCs [68,69]. In parallel, the oxidation mechanism of TCs was studied by analyzing partially electrolyzed samples with LC-QTOF-MS, aiming to understand the redox processes at the carbon SPE. Overall, the characteristic EF of TCs shown in this work enables a clear discrimination between them and other antibiotics, due to their specific electrooxidation processes. This rapid and low-cost profiling approach will ultimately allow the identification of TET, DOXY, OXY, and CHL in a decentralized manner.

2. Materials and Methods

2.1. Reagents

Tetracycline antibiotic with >91% purity was obtained from Alfa Aesar Thermo Fisher (Kandel) Germany, doxycycline hyclate purity >98% and chlortetracycline hydrochloride purity >89.5% were purchased from Acros Organics (Geel, Belgium), and oxytetracycline hydrochloride purity 95% was acquired from TCI Tokyo Chemical Industry. Phenol with purity 99% was obtained from J&K scientific GmbH, Germany. Benz[b]anthracene, N,N-dimethylcyclohexylamine and 6,11-dihydroxy-5,12-naphthacenedione, as well as all analytical grade salts of potassium chloride, sodium phosphate, sodium acetate, sodium borate, and potassium hydroxide were purchased from Sigma-Aldrich (Overijse, Belgium). All TCs stocks were prepared in 18.2 MΩ cm^{-1} doubly deionized water, except TET stock, which was prepared in ethanol, all in a concentration of 10 mM. Electrochemical measurements were performed in Britton Robinson buffer at 20 mM ionic strength with a supporting electrolyte 100 mM KCl by applying 50 µL of the buffer onto the SPE.

2.2. Instrumentation and Apparatus

All solutions were prepared in 18.2 MΩ cm^{-1} doubly deionized water (Sartorius, Arium® Ultrapure Water Systems). The pH was measured using a 913 pH meter consisting of a glass pH electrode (6.0262.100) with a reference electrolyte 3 M of KCl from Metrohm (The Netherlands).

All SWV measurements were performed using a MultiPalmSens4 or EmStat Blue potentiostats (PalmSens, The Netherlands) with PSTrace/MultiTrace or PStouch software, respectively. Disposable ItalSens IS-C graphite screen-printed electrodes (SPE) (provided by PalmSens, Utrecht, The Netherlands), containing a graphite working electrode (Ø = 3 mm), a carbon counter electrode, and a (pseudo) silver reference electrode were used for all measurements. The optimized SWV parameters: potential range of 0–1.5 V, frequency 10 Hz, 35 mV amplitude, and 5 mV step potential were used (see Supplementary Material). All the voltammograms were background corrected using the "moving average iterative background correction" (peak width = 1) tool in PSTrace software.

A custom-made script (Matlab R2018b, MathWorks, Natick, MA, USA) [68,69] was used after the analysis by SWVs to enhance peak identification. In brief, the script removes the background signal and applies a top-hat filter that provides an enhanced separation of overlapped peaks, which permits a successful identification of the TCs at pH 9 [70].

The chromatography-mass spectrometry experiments were performed on an liquid chromatograph coupled to a quadrupole time-of-flight mass spectrometer (LC-QTOF-MS) using electrospray ionization (ESI) in positive mode. The apparatus consisted of a 1290 Infinity LC (Agilent Technologies, Wilmington, DE, United States) connected to a 6530 Accurate-Mass QTOF-MS (Agilent Technologies) with a heated-ESI source (Jet-Stream ESI). Further information on the LC-QTOF-MS conditions can be found in the Supplementary Material.

3. Results and Discussions

3.1. Electrochemical Behavior of Tetracyclines via SWV

The electrochemical behavior of TCs was studied on carbon SPE in the whole pH range (2–12) using SWV. SWV was chosen because it is considered a faster and more sensitive technique, which allows for a better resolution and separation between peaks of the oxidation processes in comparison with cyclic voltammetry (CV) [71]. It is important to highlight that TCs are derived from a system of four six membered rings arranged linearly with characteristic double bonds and they have several functional groups, resulting in strong complexing properties [72]. The high similarity between structures (i.e., all TCs contain the same phenolic and di(methyl)amino substituents on position 10 and 4, respectively [73]) (Figure S1a–e) allows for an easy electrochemical discrimination from other types of antibiotics, such as amoxicillin or penicillin (see Figure 1). Therefore, it is expected that the electrochemical oxidation of the TCs will occur through the aforementioned moieties. Accordingly, two main oxidation peaks were observed in all TCs during the pH screening, with the exception of the appearance of a third oxidation process at basic pH or the merge of all the peaks at neutral pH (Figure 2). Figure 2 shows the EF of TCs (black lines), exhibiting similar electrochemical oxidation processes. Few noteworthy similarities were found between the EF in the couples TET–OXY and DOXY–CHL at pHs below 7, whereas the similarity among the couples becomes the opposite at higher pHs (TET–CHL and DOXY–OXY). As reported in the literature, TCs have variable charges on different sites, depending on the pH of the solution, because they contain three ionizable groups (tricarbonyl, dimethylammonium, and phenolic-diacetone) [10,74]. Hence, when the pH is under 4, TC exists as a cation (TCH^{3+}), due to the protonation of the dimethylammonium group (pK_a = 9.7). At a pH between 3.5 and 7.5, TC exists as a zwitterion (TCH_2^0), due to the loss of a proton from the phenolic diketone moiety (pK_a = 7.7). At a pH higher than 7, TC exists as an anion (TCH^- or TC^{2-}), due to the loss of protons from the tri-carbonyl system (pK_a = 3.3) and phenolic diketone moiety [75].

Taking into account the three ionizable groups, whole pH screening (2–12) was subsequently carried out using another four chemical compounds with similar structures (see Figure S1f–i) in order to confirm the origin of the oxidation peaks. Figure 2 summarizes the EF of the four TCs (black lines) and the other chemical compounds using the entire range of pH, and Figure S2 shows those afterward selected as optimal, pH 4 and pH 9. Benz[b]anthracene (Figure S1f) was identified as the naphthacene core shared by all TCs, thus, it was used as negative control. As expected, no oxidation peaks were observed in the EF of Figure 2 and Figure S2 (grey dashed line). Phenol (Figure S1g) directly corresponds with the phenolic substituent in position 10 (see Figure S1a), showing similar electrochemical behaviors among the EFs, as can be seen in Figure 2 and Figure S2 (blue dashed line). It is important to point out that the overlap between the EFs of phenol and the TCs was not complete in some examples, such as DOXY and CHL (see Figure 2b,d). This could be due to the presence of a chlorine atom in position 7 in the case of CHL and the absence of the hydroxyl group (–OH) at position 6 in the case of DOXY, which influences the oxidation, causing a shift towards higher potentials. Except

for this minor shift, a clear visual correlation can be observed between both EFs (phenol and TCs), which mostly coincides with the first oxidation peak of TCs in the pH screening. Subsequently, N,N-dimethylcyclohexylamine (Figure S1h) was used in the experiment, because of its tertiary amine ionizable group, to verify the origin of the second peak. As can be seen in Figure 2 and Figure S2 (red dashed line), both EFs from the corresponding TC and the N,N-dimethylcyclohexylamine overlap at pHs above 8, since the tertiary amine is protonated bellow pH 7, making its oxidation difficult [68,76]. Last but not least, the origin of a third oxidation process at higher potentials and basic pHs could be associated with the oxidation of some hydroxyl groups present in the chemical structures of TCs. To corroborate this, 6,11-dihydroxy-5,12-naphthacenedione (Figure S1i) was used, as it contains hydroxyl groups in a naphthacene core. Interestingly, the suggested oxidation of a hydroxyl group was shown as a peak at basic pHs (i.e., pH 9 to 12) (Figure 2 and Figure S2 green dashed line). Notably, the concentration of 6,11-dihydroxy-5,12-naphthacenedione was increased until 1 mM to lighten the oxidation peaks in the voltammogram (green dashed line, Figure 2 and Figure S2), while the rest of pH screenings were performed with a concentration of 10 μM. Overall, the EF of TC is enriched at basic pH, exhibiting multiple oxidation peaks attributed to the aforementioned oxidizable groups. A clear example is shown for the TC at pH 9, were the obtained EF shows three overlapped oxidation peaks. At this point, from a electrochemical point of view, the origin of the oxidation peaks exhibited in the EF of the four TCs can be confirmed.

According to the EF, the best-resolved anodic signals for oxidation of TCs on SPE were obtained at basic pHs due to the deprotonation of the oxidizable groups. However, the possibility of a dual pH approach for a selective detection of TC was parallelly considered. In particular, pH 9 was chosen as one optimal option, due to the similarities between the couples TET–CHL and DOXY–OXY, which yielded EFs with three distinguishable peaks ($P1_{TET}$ = 0.65 V, $P2_{TET}$ = 0.74 V, $P3_{TET}$ = 0.84 V and $P1_{CHL}$ = 0.64 V, $P2_{CHL}$ = 0.71 V, $P3_{CHL}$ = 0.81 V) and two peaks ($P1_{DOXY}$ = 0.65 V, $P2_{DOXY}$ = 0.77 V and $P1_{OXY}$ = 0.65 V, $P2_{OXY}$ = 0.78 V), respectively. These results differ from the previous studies reported in the literature, where the more favorable peaks always appeared at acidic pHs [54]. However, it is important to clarify that the oxidative processes and the oxidation potential may vary depending on the type of electrode, which hinders a direct comparison.

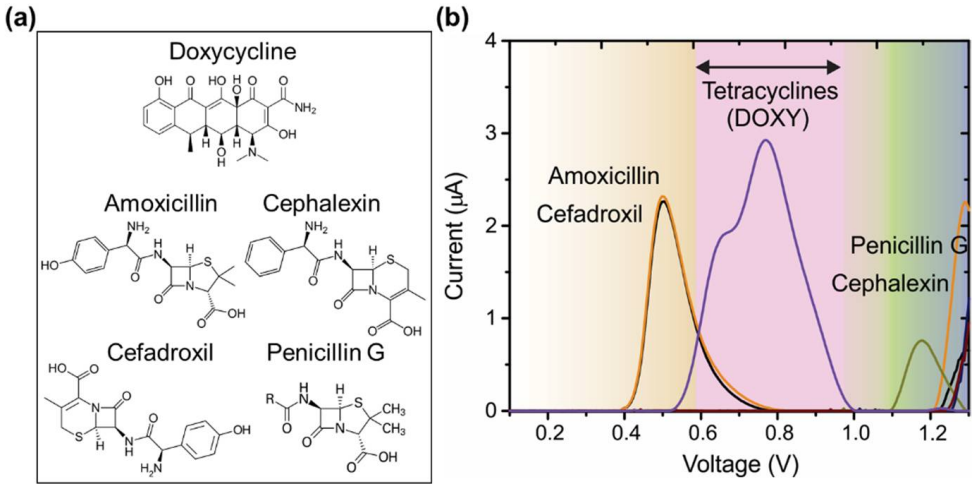

Figure 1. Comparison between (**a**) chemical structures and (**b**) peak potential range of the characteristic electrochemical fingerprints of the tetracyclines (Doxycycline, pink region) with other type of antibiotics, such as Amoxicillin and Cefadroxil (orange and grey region) or Cephalexin and Penicillin G (green and blue region). Moving average corrected square wave voltammogram using a concentration of 100 μM for each antibiotic, except for Penicillin G (1 mM).

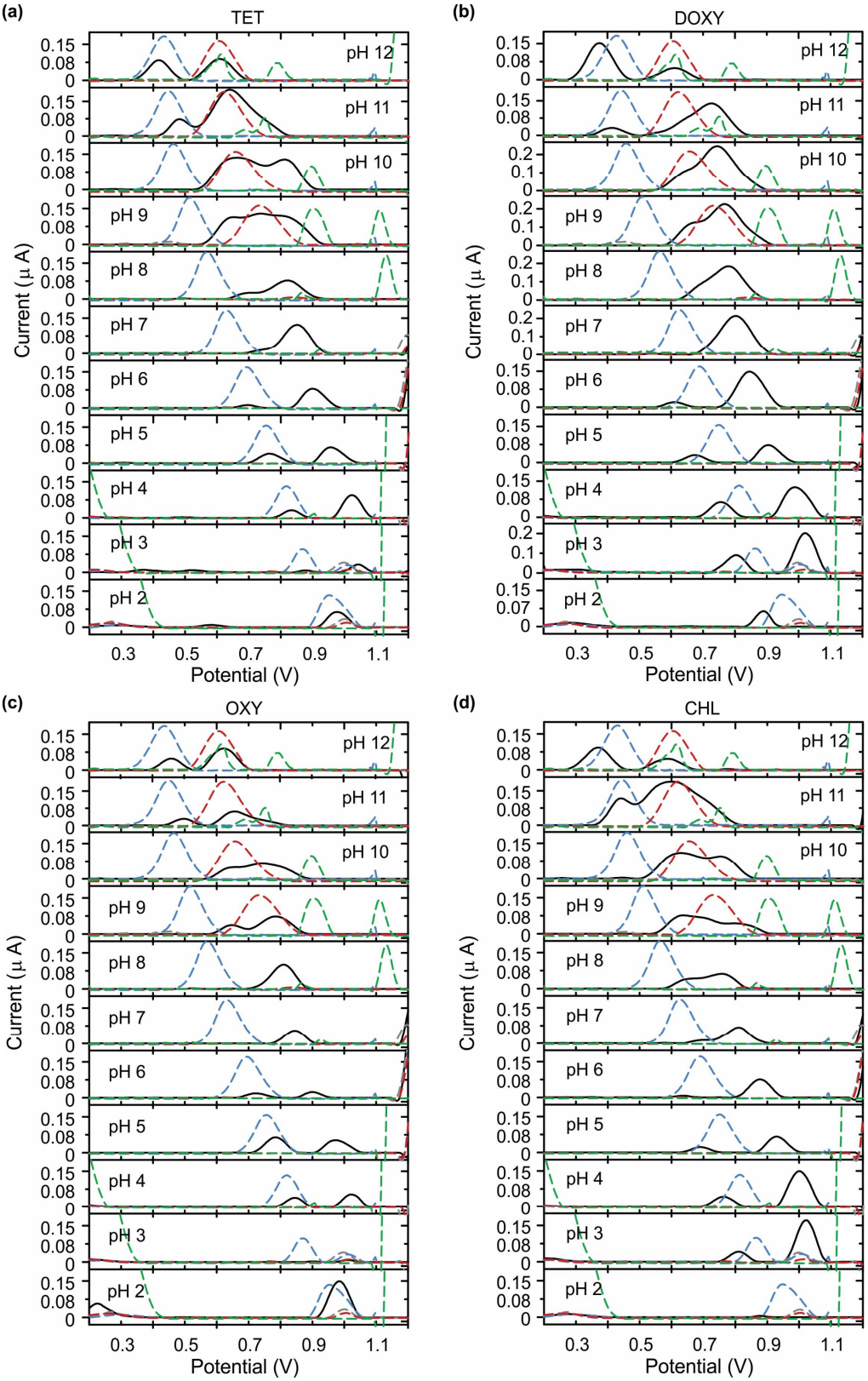

Figure 2. Square wave voltammograms (baseline-corrected) obtained in the whole pH screening range (2–12) using Britton Robinson buffer of all TCs (black line) (**a**) TET, (**b**) DOXY, (**c**) OXY, and (**d**) CHL at 10 μM concentration each. Phenol (blue dashed line), benz[b]anthracene (grey dashed line), and N,N-dimethylcyclohexylamine (red dashed line) in a concentration of 10 μM, and 6,11-dihydroxy-5,12-naphthacenedione (green dashed line) in a concentration of 1 mM.

Figure S3 shows the shift in the oxidation peak potential of TC oxidation as a function of pH (from pH 2 to 12) for the first peak corresponding to the phenol group (P1, blue squares) and the second peak corresponding to the tertiary amine group (P2, red dots). Indeed, the E_p for P1 and P2 shifts negatively with the increase of pH, which corresponds to the oxidation process of phenolic compounds and tertiary amines [73]. When a regular shift in the peak potential with pH is observed, this indicates the involvement of protons during TC oxidation reaction [40]. Some authors stated that the first peak is due to the phenol oxidation, whereas the second peak can be attributed to the oxidation of the intermediates generated during the first reaction (redox process from hydroquinone to benzoquinone) and that this can be justified because of the linear regions along the pH increment [40,73]. In this case, the linear relationship (from pH 2 to pH 12) follows a pseudo-Nernstian response in the case of the first peak (Ep $(V)_{TET} = -0.047$ pH + 1.04, Ep $(V)_{DOXY} = -0.039$ pH + 0.95, Ep $(V)_{OXY} = -0.049$ pH + 1.09, Ep $(V)_{CHL} = -0.044$ pH + 0.97), probably caused by the different overlapping of both peaks between pH 7 and 10 (see Figure S3), and a closer to Nernstian response in the case of the second peak (Ep $(V)_{TET} = -0.053$ pH + 1.22, Ep $(V)_{DOXY} = -0.039$ pH + 1.10, Ep $(V)_{OXY} = -0.049$ pH + 1.2, Ep $(V)_{CHL} = -0.059$ pH + 1.22). Interestingly, the secondary peak of CHL reaches a plateau from pH 10 to pH 12, likely due to the deprotonated tertiary amine (pK_a = 8.61). The linear relationship suggests the equal transfer of proton and electrons ($2e^-/2H^+$), matching the elucidated oxidation pathway (see Scheme 1). Interestingly, the breaks of linearity evidence that the pK_a of the different moieties was reached during the pH screening [54]. It is important to highlight that the electrodes and electrochemical approaches of the previously reported studies were different from our conditions, making it difficult to compare between the observed oxidation processes. Therefore, the elucidation of the oxidation pathway on the SPE by LC-QTOF-MS is crucial for understanding and confirming the oxidation processes (see Section 3.2).

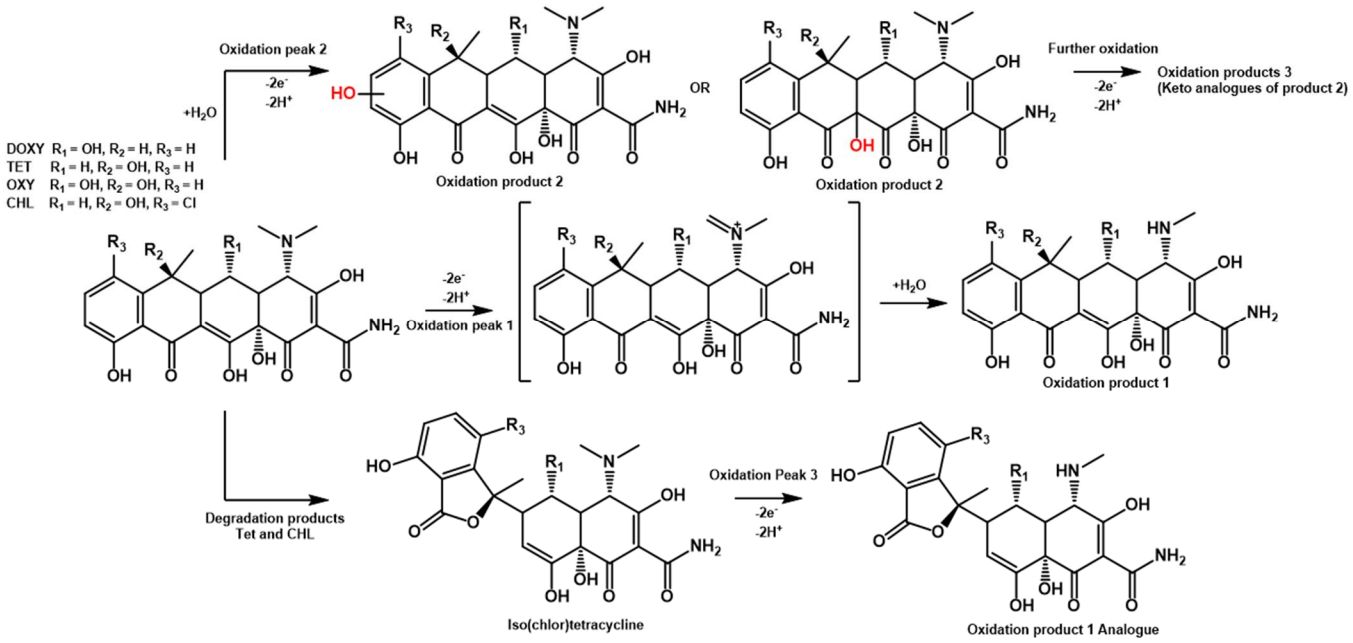

Scheme 1. Observed oxidation products in the electrochemical oxidation of tetracycline antibiotics.

3.2. Elucidation of the Oxidation Pathway of Tetracyclines via LC-QTOF-MS

Understanding the oxidation processes taking place during the voltammetric scans can play an important role in the development of efficient detection strategies [69]. Several authors have tried to explain the oxidation of different TCs through voltammetric studies; some of these are very well summarized in the work reported by Calixto et al. [54].

However, to the best of our knowledge, a profound analysis focussing on the identification of oxidation products has not yet been reported. Therefore, in order to gain an insight into the oxidation processes at the SPE and to identify possible oxidation products, TC solutions were partially electrolyzed on SPE and subsequently analysed using LC-QTOF-MS. A solution of 200 µM TCs was electrolyzed in Britton Robinson buffer pH 9 at 0.66 V and 0.85 V and in pH 4 at 0.8 V and 1.0 V. After 60 min the electrolyzed samples were diluted 1:5 with ultrapure water and directly injected into the equipment. The obtained chromatograms are compared against the standards of TCs in the same concentration, diluted 1:5. Figure 3 shows the results for DOXY, OXY, TET, and CHL (top, in black) and the three main oxidations product, all information is summarized in Table S4.

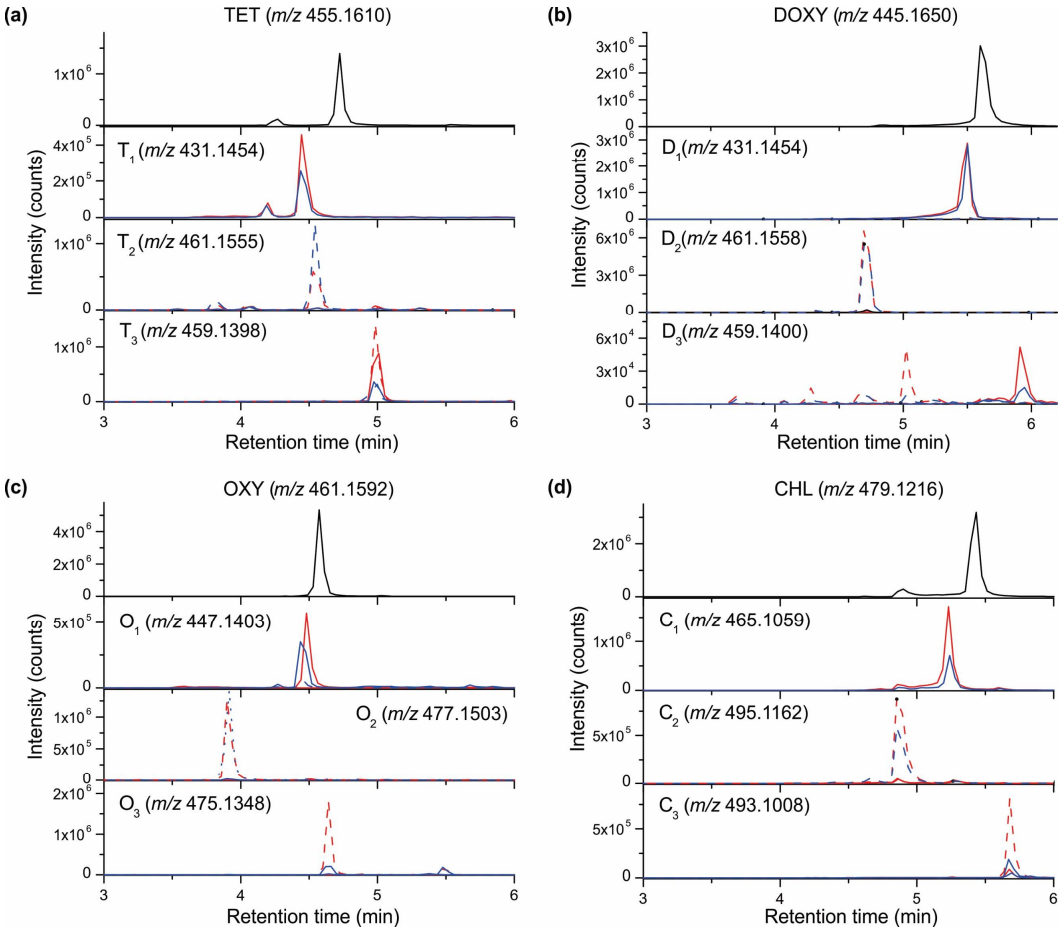

Figure 3. Extracted ion chromatogram of (**a**) TET, (**b**) DOXY, (**c**) OXY, and (**d**) CHL (diluted 1:5) and the oxidation products found after electrolysis in both Britton Robinson buffer pH 9: 0.66 V (red line) and 0.85 V (red dashed line), and pH 4: 0.8 V (blue line) and 1.0 V (blue dashed line) for 60 min.

One product was principally formed for all four TCs during the electrolysis at lower potentials, respectively 0.66 V for pH 9 and 0.80 V for pH 4. The structural information needed to suggest the structures of the oxidation products lies in these MS/MS fragmentation patterns. The key fragment in the case of the tetracyclines is "F2" (m/z 154.0498), which includes the electrochemically active tertiary amine in the tetracycline structure. In product 1 (D1, O1, T1 and C1), this F2 was not found as m/z 154.0498, but rather as 140.0340, which elutes just before the remaining non-oxidized TC with a clear loss of −14 Da, indicating the loss of a methyl-group. Surprisingly, the first electrochemical oxidation signal is not related to the phenolic-moiety of the TCs, as was previously shown by the SWV results, but rather the oxidation of the tertiary-amine group. During the oxidation process, the tertiary amine is oxidatively converted to a secondary amine. This was confirmed by

comparing the MSMS spectra of DOXY (Figure S4a) and the oxidation products D_1 and D_2 (Figure S4b,c). Not only the mother-ion $[M + H]^+$ of product D1 exhibits a clear loss of the 14 Da compared to DOXY (*m/z* 431.1454 *versus m/z* 445.1603, see Table S4), but it can also be seen in the typical fragment of *m/z* 154.0498 of DOXY observed in product D1 as *m/z* 140.0430 (Figure S4a,b), corresponding with the loss of a methyl-group. Moreover, the fragment that indicates the presence of the tertiary amine group, *m/z* 58.0657 ($[C_3H_8N]^+$), could not be observed for D_1, while other fragments such as *m/z* 321.075 ($[C_{19}H_{13}O_5]^+$) and *m/z* 267.065 ($[C_{16}H_{11}O_4]^+$) are identical to DOXY as they do not contain any nitrogen atoms.

For the electrolysis at higher potentials, namely 0.85 V for pH 9 and 1.00 V pH 4, a second main oxidation product was formed (D_2, O_2, T_2 and C_2, Figure 3 and Table S4), while the products of the first oxidation peak had almost completely disappeared. When the molecular ion masses of the products are compared to the corresponding non-oxidized TC, a clear addition of 16 Da is observed for all TCs, indicating that an additional oxygen is incorporated into the structure. Based on the MSMS fragmentation pattern of D_2 this addition does not take place close to the tertiary amine group, as the fragment *m/z* 154.0498 can still be observed. Therefore, this product is formed during the oxidation of the phenolic-moiety in the DOXY, and the same conclusion is attributed to the rest of the TCs. On the other hand, it is extremely difficult to assign a specific position to the additional hydroxyl-group in this product based on the LC-QTOF-MS analysis alone. In the literature, for oxidative degradation of tetracyclines this is sometimes suggested to be at either the para, meta, or ortho-position of the phenolic-group (OH groups indicated in red in Scheme 1), whereas other articles suggest a similar product as for the enzymatic oxidation of tetracyclines [16,77–79]. Herein, it is known that the oxidative addition takes place at the 11a position. At these higher potentials the newly formed incorporated hydroxyl-group can be even oxidized, resulting in a keto analogue of the second oxidation product, which corresponds to the remaining oxidation products D_3, O_3, T_3, and C_3 (Figure 3, Table S4). However, this does not explain the appearance of the third oxidation peak previously shown only for TET and CHL (Figure 2). However, the answer lies in the occurrence of a second peak in the chromatogram at 4.72 min (*m/z* 445.1605) and 5.44 min (*m/z* 479.1233) of the standards of TET and CHL, respectively. These products possess the same *m/z*-value as the TC itself, meaning that they are rearranged degradation products specific to these TC. It has been reported for TET and CHL that these two TCs are particularly sensitive to the formation of iso(chlor)tetracycline [80]. Therefore, the formation of isotetracycline is the most likely explanation for this part of the study and was also shown to be electroactive by the HPLC coupled to an electrochemical detector (Figure S5). These results correlate with the third oxidation peak observed throughout the SWV analysis. Hence, the redox pathway suggested for the oxidation of tetracycline antibiotics is exhibited in Scheme 1.

3.3. Calibration Curves

A preliminary optimization was carried out before performing the calibration curve at pH 9 to test the analytical performance of the sensor towards different TCs (Figure 4). First, the influence of supporting electrolytes (potassium chloride, KCl) on the electrochemical response was initially studied at pH 2 (Figure S6), showing an oxidation peak at ca. 0.95 V corresponding to the oxidation of the phenolic moiety. Hence, 100 mM KCl was selected as an optimal concentration for further experiments. Moreover, the optimization of the SWV parameters—step potential (E step), amplitude, and frequency—was carried out (see Figure S7). As a result, an E step of 5 mV, amplitude of 35 mV, and frequency of 10 Hz were chosen as optimal conditions to obtain the best performance regarding the peak intensity, better signal-to-noisy ratio, and/or the best adaptation to the specific software for data treatment (Matlab script). Figure 4a–d displays the SW voltammograms of the TCs upon increasing concentrations. Accordingly, Figure 4e–h exhibits the corresponding calibration curves, with the calculated analytical parameters shown in Table 1. Subsequently, the reproducibility ($N = 3$) of the SWV of the TCs at pH 9 in a concentration of 10 μM, as well as the stability of the stock solutions (from 1 to 3 weeks) at pH 9 to test its possible degradation

over time in the alkaline solution, were evaluated (Figures S8 and S9, respectively). The results show excellent reproducibility, with RSD < 10% (Table 1). Moreover, negligible degradation of DOXY, OXY, and CHL solution stocks in pH 9 was observed over time (more than 3 weeks period), showing RSD values (N = 3) of 5.04%, 5.72%, and 5.15%, respectively. On the other hand, TET exhibits higher degradation after the first week with an RSD of 20.23% (N = 3), consistent with the change in color (from yellow to red) and the appearance of precipitates.

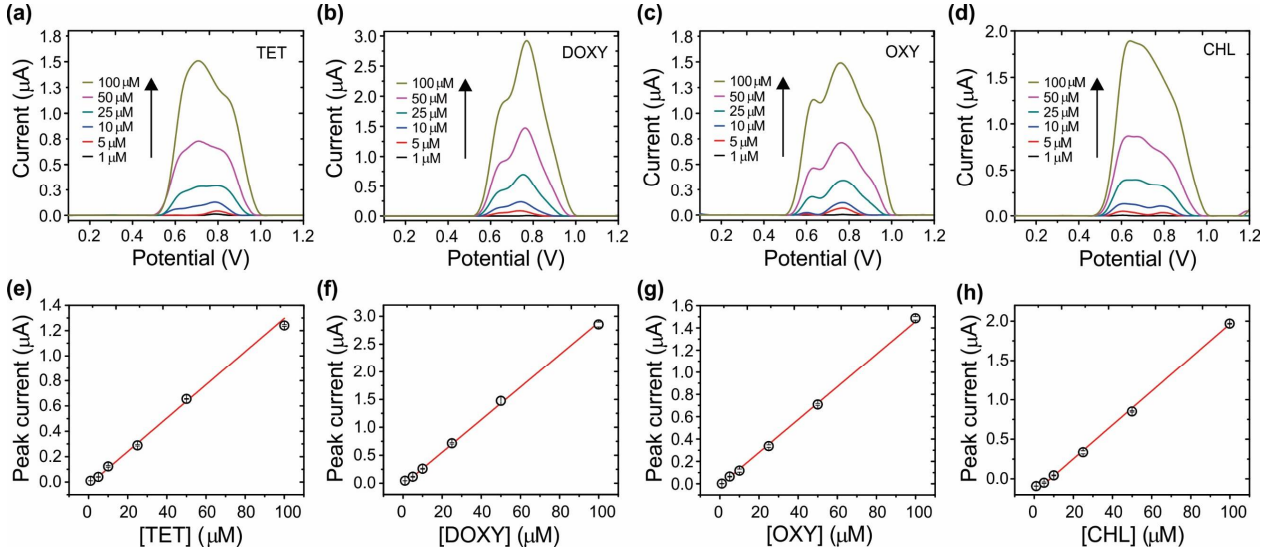

Figure 4. Baseline-corrected SWV for (**a**) TET, (**b**) DOXY, (**c**) OXY, and (**d**) CHL at pH 9 in Britton Robinson buffer in a range from 1 to 100 μM using carbon SPE. Corresponding calibration curves of the four TCs (**e**) TET, (**f**) DOXY, (**g**) OXY, and (**h**) CHL showing the peak current versus concentration of the different TCs (N = 3).

Table 1. Analytical parameters obtained from calibrations curves of TET, DOXY, OXY, and CHL in a range from 1 to 100 μM concentration and RDS obtained from the reproducibility study (Figure S8).

	TET	DOXY	OXY	CHL
Sensitivity (μA μM^{-1})	0.013	0.030	0.015	0.020
R-squared	0.998	0.999	0.999	0.999
Linear range (μM)	5–100	5–100	5–100	5–100
Limit of detection (μM)	4.17	2.14	3.07	2.49
RSD (%) at 10 μM, N = 3	3.01	3.29	9.78	6.88

3.4. Data Treatment towards an Enhanced Peak Analysis

A Matlab script was designed to improve the identification of the oxidation peaks in the EF [68,69]. In particular, for the cases in which the overlapping of signals creates shoulders and tails in the peak, the aforementioned tool improves the peak separation, and thus the peak identification, allowing for a trustworthy compound identification based on the characteristic oxidation processes of the EF [70]. Hence, the script was implemented for all the EF obtained during the pH screening. After studying the general behavior of the TCs at different pHs, two pHs exhibited a characteristic enrichment of the EFs: *(i)* pH 9 showed high peak intensity and interesting EF similarities (same E_p) between the couples TET–CHL (with three peaks, $P1_{TET}$ = 0.65 V, $P2_{TET}$ = 0.74 V, $P3_{TET}$ = 0.84 V and $P1_{CHL}$ = 0.64 V, $P2_{CHL}$ = 0.71 V, $P3_{CHL}$ = 0.81 V) and DOXY–OXY (in contrast showing two peaks, $P1_{DOXY}$ = 0.65 V, $P2_{DOXY}$ = 0.77 V and $P1_{OXY}$ = 0.65 V, $P2_{OXY}$ = 0.78 V, respectively), and *(ii)* pH 4 due to the easy identification between the peak potentials of two different couples of TCs, TET–OXY ($P1_{TET}$ = 0.84 V, $P2_{TET}$ = 1.02 V, $P1_{OXY}$ = 0.85 V, $P2_{OXY}$ = 1.02 V) and DOXY–CHL ($P1_{DOXY}$ = 0.75 V, $P2_{DOXY}$ = 0.99 V, $P1_{CHL}$ = 0.76 V, $P2_{CHL}$ = 1 V). Therefore,

a dual pH strategy might permit the selective determination of specific TCs based on the EF in an unknown sample.

Figure 5 summarizes the comparison of SWVs obtained from the potentiostat software (i.e., baseline corrected by moving average correction), and after employing data analysis (i.e., tailor-made script) of the four TCs at pH 4 and pH 9. The script did not improve the peak separation for pH 4 (Figure 5a–b). On the contrary, the script was crucial to elucidate the number of peaks at pH 9 that potentially correspond to different oxidation processes. Figure 5c shows the SWVs of TCs that clearly exhibit shoulders on oxidation peaks corresponding to partially overlaying signals of different electroactive groups. After data analysis (Figure 5d), an improved peak separation was accomplished, allowing for an easy identification of the specific EF for each TC, showing three peaks in the case of TET and CHL, and only two peaks in the case of DOXY and OXY. Therefore, at this point, a two-step protocol was established for the determination of TET, DOXY, OXY, and CHL: (*i*) a preliminary screening at pH 4 to obtain a first identification between two different couples (TET–OXY or CHL–DOXY), followed by (*ii*) a confirmatory screening at pH 9 to elucidate the specific TC present in the sample, taking advantage of the similarities between the different couples (three peaks in the couple TET–CHL and two peaks in DOXY–OXY).

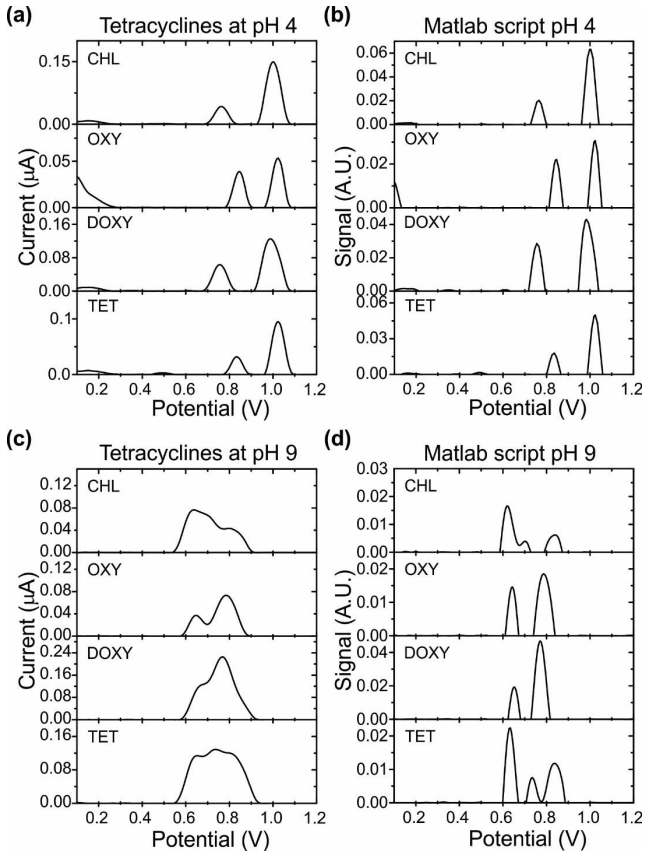

Figure 5. Data treatment with Matlab script to improve peak separation/identification. (**a**) Baseline-corrected SWVs of tetracyclines at pH 4, (**b**) output signal after the application of the script at pH 4, (**c**) baseline-corrected SWVs of TCs at pH 9, where overlapping of peaks exists, and (**d**) output signal after the application of the script at pH 9.

3.5. Single, Binary, Tertiary, and Complex Mixtures of TCs

The aim of the proposed approach was not just being able to distinguish TCs among other antibiotics (which was successfully shown in Figure 1), but also between themselves, and thus to identify possible overlapping and suppression effects, which could lead to false positive and false negative results, respectively. Therefore, apart from being able to detect

single TCs in an unknown sample, the next step was to analyze if different TCs could be identified in binary, tertiary, or quaternary mixtures. Figure S10 shows another example where all TCs in different mixtures at pH 9 can be compared between the SWVs obtained from the potentiostat software (i.e., moving average correction), and after employing data analysis (i.e., tailor-made script), which facilitates the separation between peaks. It is worth mentioning that the treated signal after the script does not correspond to the current intensity of the SWVs, thus producing signals for a qualitative analysis.

Figure 6 displays the whole summary of single, binary, tertiary, and quaternary combinations of the four studied TCs at pH 4 (Figure 6a) and pH 9 (Figure 6b). A dashed line color code has been added to facilitate the identification of the TC present in the corresponding mixture, i.e., orange for TET, green for DOXY, blue for OXY, and purple for CHL. As can be seen from the figure, if a single TC is present in the sample, the identification can be successfully achieved (green tick) by the dual pH strategy and the Matlab script (only required at pH 9, see Figure S10). As a practical example, if an EF showing two peaks at 0.82 V and 1.1 V is obtained at pH 4, one could easily identify the presence of TET or OXY. Afterwards, a second SWV at pH 9 is carried out to confirm which TC is present in the sample. Therefore, the appearance of two peaks (after Matlab script) at 0.63 V and 0.79 V means that the TC present in the sample is OXY.

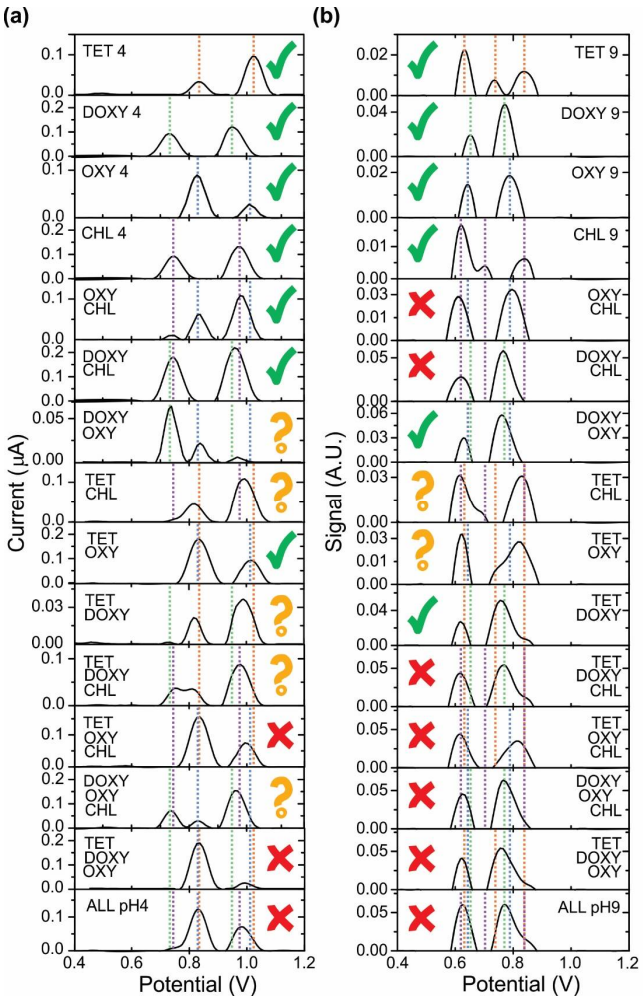

Figure 6. Electrochemical fingerprint of TCs in all type of combinations and mixtures at (**a**) pH 4, SWVs raw data (moving average correction) and (**b**) pH 9, output signal after the application of the script. The successful recognition of the TC is represented in the figure with a green tick (√), followed by an orange question mark (?) or a red cross (X) for inconclusive and unsuccessful identifications, respectively.

After the binary mixtures are introduced, the complexity of the exercise increases, making possible a proper identification in some cases (i.e., DOXY + OXY and TET + DOXY, Figure 6b). Other mixtures lead to inconclusive results (orange question mark), such as TET + CHL and TET + OXY, where the middle peaks corresponding to CHL and TET appear with a slight shoulder after applying the Matlab script, instead of being clearly separated. Unfortunately, tertiary and quaternary mixtures of TCs were very difficult to determine (red cross). Future steps will consider a deeper exploration and optimization in both the electrochemical setup and the Matlab script. Nevertheless, it is important to again point out that although the identification becomes challenging upon increasing the complexity of the mixtures, it is still possible to distinguish the entire class of TCs from other types of antibiotics (Figure 1).

4. Conclusions

This work reveals, for the first time, a complete study of the electrochemistry of four different tetracyclines (TC) antibiotics: tetracycline (TET), doxycycline (DOXY), oxytetracycline (OXY), and chlortetracycline (CHL). The aim of the present manuscript was to collect detailed information about the oxidation processes of these TCs from both electrochemical and chromatographic points of view, in order to clarify the reactions and pave the way towards the development of more accurate and reliable detection platforms. Furthermore, a broad overview of the previously reported electrochemical sensors and biosensors based on surface modification, aptamers, antibodies, enzymes, or MIP for TC determination was included. From the electrochemical section, the electrochemical fingerprint of the tetracyclines in the whole pH range (from 2 to 12) was studied via SWV on unmodified carbon SPEs. Moreover, the main oxidation processes were attributed to the corresponding electroactive groups (i.e., phenol, tertiary amine, and hydroxyl groups) by comparing the electrochemical behavior of TCs with different chemical compounds sharing similar moieties. In addition, a successful protocol for the identification of a single TC in unknown samples was developed based on a dual pH strategy and an innovative custom-made script designed to enhance the separation between oxidation peaks. Subsequently, from a chromatographic perspective, the oxidation mechanism of the TCs was elucidated for the first time by LC-QTOF-MS and different oxidation products were clearly detected and identified after the electrolysis at SPE. Overall, this work encompasses relevant information about the electrochemical behavior of TCs and points out a simple, rapid, and reliable electrochemical approach for the identification of tetracycline antibiotics in combination with a custom Matlab script. The present work aims to pave the way and bring new insights towards the development of future analytical platforms for the reliable determination of antibiotics in decentralized settings.

Supplementary Materials: The following are available online at https://www.mdpi.com/article/10.3390/chemosensors9070187/s1, LC-QTOF-MS Conditions, Figure S1. Chemical structure of the tetracycline antibiotics, Figure S2. pH screening (2–12) for all tetracyclines, Figure S3. Peak potential *versus* pH, Figure S4. MS/MS spectra of DOXY, Figure S5. HPLC–ECD chromatograms of TCs at 10 μM, Figure S6. Electrochemical influence of the supporting electrolyte, Figure S7. Optimization of the main parameters used in SWV, Figure S8. Reproducibility study, Figure S9. Stability study, Figure S10. Output signal after the utilization of the script, Table S1. Maximum residue limit (MRL) for tetracyclines in animal tissues, Table S2. Summary of electrochemical biosensors based on aptamers, antibodies, molecular imprinted polymers and enzyme-linked immunoassays for tetracyclines (TCs) detection, Table S3. Summary of electrochemical approaches based on modified electrodes for tetracycline determination, Table S4. LC-QTOF data for all four TCs and the three main oxidation products.

Author Contributions: R.C.: Conceptualization, Data curation, Formal analysis, Investigation, Methodology, Validation, Visualization, Writing—original draft, drafting the article and revising it critically for important intellectual content. N.S.: Data curation, Formal analysis, Investigation. A.L.N.v.N.: Resources, Writing—final approval of the version to be submitted. K.D.W.: Funding acquisition, Methodology, Resources, Supervision, Project administration, Writing—final approval

of the version to be submitted. All authors have read and agreed to the published version of the manuscript.

Funding: FWO (Research Foundation—Flanders) grant number G054819N, 2018.

Institutional Review Board Statement: Not applicable.

Informed Consent Statement: Not applicable.

Data Availability Statement: Not applicable.

Acknowledgments: The authors would like to acknowledge the financial support from FWO (Research Foundation—Flanders, grant number G054819N, 2018) and the financial support from the University of Antwerp.

Conflicts of Interest: The authors declare no conflict of interest.

References

1. Oka, H.; Ito, Y.; Matsumoto, H. Chromatographic analysis of tetracycline antibiotics in foods. *J. Chromatogr. A* **2000**, *882*, 109–133. [CrossRef]
2. Masawat, P.; Slater, J.M. The determination of tetracycline residues in food using a disposable screen-printed gold electrode (SPGE). *Sens. Actuators B Chem.* **2007**, *124*, 127–132. [CrossRef]
3. Le, T.H.; Pham, V.P.; La, T.H.; Phan, T.B.; Le, Q.H. Electrochemical aptasensor for detecting tetracycline in milk. *Adv. Nat. Sci. Nanosci. Nanotechnol.* **2016**, *7*. [CrossRef]
4. Zhao, F.; Zhang, X.; Gan, Y. Determination of tetracyclines in ovine milk by high-performance liquid chromatography with a coulometric electrode array system. *J. Chromatogr. A* **2004**, *1055*, 109–114. [CrossRef]
5. Liu, X.; Huang, D.; Lai, C.; Zeng, G.; Qin, L.; Zhang, C.; Yi, H.; Li, B.; Deng, R.; Liu, S.; et al. Recent advances in sensors for tetracycline antibiotics and their applications. *TrAC Trends Anal. Chem.* **2018**, *109*, 260–274. [CrossRef]
6. Palaharn, S.; Charoenraks, T.; Wangfuengkanagul, N.; Grudpan, K.; Chailapakul, O. Flow injection analysis of tetracycline in pharmaceutical formulation with pulsed amperometric detection. *Anal. Chim. Acta* **2003**, *499*, 191–197. [CrossRef]
7. Brodersen, D.E.; Clemons, W.M.; Carter, A.P.; Morgan-Warren, R.J.; Wimberly, B.T.; Ramakrishnan, V. The structural basis for the action of the antibiotics tetracycline, pactamycin, and hygromycin B, on the 30S ribosomal subunit. *Cell* **2000**, *103*, 1143–1154. [CrossRef]
8. Liu, X.; Zheng, S.; Hu, Y.; Li, Z.; Luo, F.; He, Z. Electrochemical Immunosensor Based on the Chitosan-Magnetic Nanoparticles for Detection of Tetracycline. *Food Anal. Methods* **2016**, *9*, 2972–2978. [CrossRef]
9. Pellegrini, G.E.; Carpico, G.; Coni, E. Electrochemical sensor for the detection and presumptive identification of quinolone and tetracycline residues in milk. *Anal. Chim. Acta* **2004**, *520*, 13–18. [CrossRef]
10. Kim, Y.J.; Kim, Y.S.; Niazi, J.H.; Gu, M.B. Electrochemical aptasensor for tetracycline detection. *Bioprocess Biosyst. Eng.* **2010**, *33*, 31–37. [CrossRef]
11. Casella, I.G.; Fabio, P. Determination of tetracycline residues by liquid chromatography coupled with electrochemical detection and solid phase extraction. *J. Agric. Food Chem.* **2009**, *57*, 8735–8741. [CrossRef]
12. Rudnicki, K.; Sipa, K.; Brycht, M.; Borgul, P.; Skrzypek, S.; Poltorak, L. Electrochemical sensing of fluoroquinolone antibiotics. *TrAC Trends Anal. Chem.* **2020**, *128*, 115907. [CrossRef]
13. Shen, G.; Guo, Y.; Sun, X.; Wang, X. Electrochemical Aptasensor Based on Prussian Blue-Chitosan-Glutaraldehyde for the Sensitive Determination of Tetracycline. *Nano-Micro Lett.* **2014**, *6*, 143–152. [CrossRef]
14. Pastor-Navarro, N.; Morais, S.; Maquieira, Á.; Puchades, R. Synthesis of haptens and development of a sensitive immunoassay for tetracycline residues. Application to honey samples. *Anal. Chim. Acta* **2007**, *594*, 211–218. [CrossRef]
15. Faridah, S.; Azura, N.; Hazana, R.; Gayah, A.R.; Norzaili, Z.; Azima, A.; Zamri, I. Electrochemical sensors for detection of tetracycline antibiotics Unbound free tetracycline and tetracycline conjugates were removed during the washing step Direct competitive ELISA method Carbon working electrode was connected to the electrochemical ayse. *Malays. Soc. Anim. Prod.* **2012**, *15*, 67–80.
16. Zhi, D.; Qin, J.; Zhou, H.; Wang, J.; Yang, S. Removal of tetracycline by electrochemical oxidation using a Ti/SnO_2–Sb anode: Characterization, kinetics, and degradation pathway. *J. Appl. Electrochem.* **2017**, *47*, 1313–1322. [CrossRef]
17. Vega, D.; Agüí, L.; González-Cortés, A.; Yáñez-Sedeño, P.; Pingarrón, J.M. Voltammetry and amperometric detection of tetracyclines at multi-wall carbon nanotube modified electrodes. *Anal. Bioanal. Chem.* **2007**, *389*, 951–958. [CrossRef]
18. Zhu, J.; Snow, D.D.; Cassada, D.A.; Monson, S.J.; Spalding, R.F. Analysis of oxytetracycline, tetracycline, and chlortetracycline in water using solid-phase extraction and liquid chromatography-tandem mass spectrometry. *J. Chromatogr. A* **2001**, *928*, 177–186. [CrossRef]
19. Hayat, A.; Marty, J.L. Aptamer based electrochemical sensors for emerging environmental pollutants. *Front. Chem.* **2014**, *2*, 1–9. [CrossRef] [PubMed]
20. Dos Santos, A.J.; Kronka, M.S.; Fortunato, G.V.; Lanza, M.R.V. Recent advances in electrochemical water technologies for the treatment of antibiotics: A short review. *Curr. Opin. Electrochem.* **2021**, *26*, 100674. [CrossRef]

21. Wong, A.; Scontri, M.; Materon, E.M.; Lanza, M.R.V.; Sotomayor, M.D.P.T. Development and application of an electrochemical sensor modified with multi-walled carbon nanotubes and graphene oxide for the sensitive and selective detection of tetracycline. *J. Electroanal. Chem.* **2015**, *757*, 250–257. [CrossRef]
22. Hayat, A.; Marty, J.L. Disposable screen printed electrochemical sensors: Tools for environmental monitoring. *Sensors* **2014**, *14*, 10432–10453. [CrossRef]
23. Feng, Y.; Yan, T.; Wu, T.; Zhang, N.; Yang, Q.; Sun, M.; Yan, L.; Du, B.; Wei, Q. A label-free photoelectrochemical aptasensing platform base on plasmon Au coupling with MOF-derived In_2O_3@g-C_3N_4 nanoarchitectures for tetracycline detection. *Sens. Actuators B Chem.* **2019**, *298*, 126817. [CrossRef]
24. Guo, Y.; Wang, X.; Sun, X. A label-free electrochemical aptasensor based on electrodeposited gold nanoparticles and methylene blue for tetracycline detection. *Int. J. Electrochem. Sci.* **2015**, *10*, 3668–3679.
25. Alawad, A.; Istamboulié, G.; Calas-Blanchard, C.; Noguer, T. A reagentless aptasensor based on intrinsic aptamer redox activity for the detection of tetracycline in water. *Sens. Actuators B Chem.* **2019**, *288*, 141–146. [CrossRef]
26. Taghdisi, S.M.; Danesh, N.M.; Ramezani, M.; Abnous, K. A novel M-shape electrochemical aptasensor for ultrasensitive detection of tetracyclines. *Biosens. Bioelectron.* **2016**, *85*, 509–514. [CrossRef]
27. Piaopiao, C.; Yichen, X.; Xiaoxiao, C.; Shan, Z.; Yang, L.; Chaobiao, H. A "Signal On" Photoelectrochemical Aptasensor For Tetracycline Detection Based On Semiconductor Polymer Quantum Dots. *J. Electrchem. Soc.* **2020**, *167*, 067516. [CrossRef]
28. Zarei, M. Sensitive visible light-driven photoelectrochemical aptasensor for detection of tetracycline using ZrO_2/g-C_3N_4 nanocomposite. *Sens. Int.* **2020**, *1*, 100029. [CrossRef]
29. Yang, Y.; Yan, W.; Guo, Y.; Wang, X.; Zhang, F.; Yu, L.; Guo, C.; Fang, G. Sensitive and selective electrochemical aptasensor via diazonium-coupling reaction for label-free determination of oxytetracycline in milk samples. *Sens. Actuators Rep.* **2020**, *2*, 100009. [CrossRef]
30. Hu, X.; Xu, Y.; Cui, X.; Li, W.; Huang, X.; Li, Z.; Shi, J.; Zou, X. Fluorometric and electrochemical dual-mode nanoprobe for tetracycline by using a nanocomposite prepared from carbon nitride quantum dots and silver nanoparticles. *Microchim. Acta* **2020**, *187*, 1–10. [CrossRef]
31. Zhang, J.; Wu, Y.; Zhang, B.; Li, M.; Jia, S.; Jiang, S.; Zhou, H.; Zhang, Y.; Zhang, C.; Turner, A.P.F. Label-Free Electrochemical Detection of Tetracycline by an Aptamer Nano-Biosensor. *Anal. Lett.* **2012**, *45*, 986–992. [CrossRef]
32. Zhou, L.; Li, D.J.; Gai, L.; Wang, J.P.; Li, Y. Bin Electrochemical aptasensor for the detection of tetracycline with multi-walled carbon nanotubes amplification. *Sens. Actuators B Chem.* **2012**, *162*, 201–208. [CrossRef]
33. Jeon, M.; Kim, J.; Paeng, K.J.; Park, S.W.; Paeng, I.R. Biotin-avidin mediated competitive enzyme-linked immunosorbent assay to detect residues of tetracyclines in milk. *Microchem. J.* **2008**, *88*, 26–31. [CrossRef]
34. Zhang, Y.; Lu, S.; Liu, W.; Zhao, C.; Xi, R. Preparation of anti-tetracycline antibodies and development of an indirect heterologous competitive enzyme-linked immunosorbent assay to detect residues of tetracycline in milk. *J. Agric. Food Chem.* **2007**, *55*, 211–218. [CrossRef] [PubMed]
35. Devkota, L.; Nguyen, L.T.; Vu, T.T.; Piro, B. Electrochemical determination of tetracycline using AuNP-coated molecularly imprinted overoxidized polypyrrole sensing interface. *Electrochim. Acta* **2018**, *270*, 535–542. [CrossRef]
36. Wang, H.; Zhao, H.; Quan, X.; Chen, S. Electrochemical Determination of Tetracycline Using Molecularly Imprinted Polymer Modified Carbon Nanotube-Gold Nanoparticles Electrode. *Electroanalysis* **2011**, *23*, 1863–1869. [CrossRef]
37. Jampasa, S.; Pummoree, J.; Siangproh, W.; Khongchareonporn, N.; Bgamrojanavanich, N.; Chailapakul, O.; Chaiyo, S. Chemical "Signal-On" electrochemical biosensor based on a competitive immunoassay format for the sensitive determination of oxytetracycline. *Sens. Actuators B. Chem.* **2020**, *320*, 128389. [CrossRef]
38. Starzec, K.; Cristea, C.; Tertis, M.; Feier, B.; Wieczorek, M.; Koscielniak, P.; Kochana, J. Employment of electrostriction phenomenon for label-free electrochemical immunosensing of tetracycline. *Bioelectrochemistry* **2020**, *132*, 107405. [CrossRef]
39. El Alami El Hassani, N.; Baraket, A.; Boudjaoui, S.; Taveira Tenório Neto, E.; Bausells, J.; El Bari, N.; Bouchikhi, B.; Elaissari, A.; Errachid, A.; Zine, N. Development and application of a novel electrochemical immunosensor for tetracycline screening in honey using a fully integrated electrochemical Bio-MEMS. *Biosens. Bioelectron.* **2019**, *130*, 330–337. [CrossRef]
40. Kushikawa, R.T.; Silva, M.R.; Angelo, A.C.D.; Teixeira, M.F.S. Construction of an electrochemical sensing platform based on platinum nanoparticles supported on carbon for tetracycline determination. *Sens. Actuators B Chem.* **2016**, *228*, 207–213. [CrossRef]
41. Luo, Y.; Xu, J.; Li, Y.; Gao, H.; Guo, J.; Shen, F.; Sun, C. A novel colorimetric aptasensor using cysteamine-stabilized gold nanoparticles as probe for rapid and specific detection of tetracycline in raw milk. *Food Control* **2015**, *54*, 7–15. [CrossRef]
42. Chen, B.; Zhang, Z.; Sun, X.; Kuang, Y.; Mao, X.; Wang, X.; Yan, Z.; Li, B.; Xu, Y.; Yu, M.; et al. Biallelic Mutations in PATL2 Cause Female Infertility Characterized by Oocyte Maturation Arrest. *Am. J. Hum. Genet.* **2017**, *101*, 609–615. [CrossRef] [PubMed]
43. Xu, Q.; Liu, Z.; Fu, J.; Zhao, W.; Guo, Y.; Sun, X.; Zhang, H. Ratiometric electrochemical aptasensor based on ferrocene and carbon nanofibers for highly specific detection of tetracycline residues. *Sci. Rep.* **2017**, *7*, 14729. [CrossRef] [PubMed]
44. Zhan, X.; Hu, G.; Wagberg, T.; Zhan, S.; Xu, H.; Zhou, P. Electrochemical aptasensor for tetracycline using a screen-printed carbon electrode modified with an alginate film containing reduced graphene oxide and magnetite (Fe_3O_4) nanoparticles. *Microchim. Acta* **2016**, *183*, 723–729. [CrossRef]
45. Shi, Z.; Hou, W.; Jiao, Y.; Guo, Y.; Sun, X.; Zhao, J.; Wang, X. Ultra-sensitive aptasensor based on IL and Fe_3O_4 nanoparticles for tetracycline detection. *Int. J. Electrochem. Sci.* **2017**, *12*, 7426–7434. [CrossRef]

46. Jahanbani, S.; Benvidi, A. Comparison of two fabricated aptasensors based on modified carbon paste/oleic acid and magnetic bar carbon paste/Fe_3O_4@oleic acid nanoparticle electrodes for tetracycline detection. *Biosens. Bioelectron.* **2016**, *85*, 553–562. [CrossRef]
47. Munteanu, F.D.; Titoiu, A.M.; Marty, J.L.; Vasilescu, A. Detection of antibiotics and evaluation of antibacterial activity with screen-printed electrodes. *Sensors* **2018**, *18*, 901. [CrossRef]
48. Han, Q.; Wang, R.; Xing, B.; Chi, H.; Wu, D.; Wei, Q. Label-free photoelectrochemical aptasensor for tetracycline detection based on cerium doped CdS sensitized BiYWO6. *Biosens. Bioelectron.* **2018**, *106*, 7–13. [CrossRef]
49. Lorenzetti, A.S.; Sierra, T.; Domini, C.E.; Lista, A.G.; Crevillen, A.G.; Escarpa, A. Electrochemically Reduced Graphene Oxide-Based Screen-Printed Electrodes for Total Tetracycline Determination by Adsorptive Transfer Stripping. *Sensors* **2020**, *20*, 76. [CrossRef]
50. Mohammad-Razdari, A.; Ghasemi-Varnamkhasti, M.; Rostami, S.; Izadi, Z.; Ensafi, A.A.; Siadat, M. Development of an electrochemical biosensor for impedimetric detection of tetracycline in milk. *J. Food Sci. Technol.* **2020**, *57*, 4697–4706. [CrossRef] [PubMed]
51. Tang, Y.; Liu, P.; Xu, J.; Li, L.; Yang, L.; Liu, X.; Liu, S.; Zhou, Y. Electrochemical aptasensor based on a novel flower-like TiO_2 nanocomposite for the detection of tetracycline. *Sens. Actuators B Chem.* **2018**, *258*, 906–912. [CrossRef]
52. Calixto, C.M.F.; Cavalheiro, É.T.G. Determination of Tetracycline in Bovine and Breast Milk Using a Graphite–Polyurethane Composite Electrode. *Anal. Lett.* **2017**, *50*, 2323–2334. [CrossRef]
53. Abraham, T.; Gigimol, M.G.; Priyanka, R.N.; Susan, M.; Korah, B.K.; Mathew, B. In-situ fabrication of Ag_3PO_4 based binary composite for the efficient electrochemical sensing of tetracycline. *Mater. Lett.* **2020**, *279*, 128502. [CrossRef]
54. Calixto, C.M.F.; Cervini, P.; Cavalheiro, É.T.G. Determination of tetracycline in environmental water samples at a graphite-polyurethane composite electrode. *J. Braz. Chem. Soc.* **2012**, *23*, 938–943. [CrossRef]
55. Calixto, C.M.F.; Cavalheiro, É.T.G. Determination of Tetracyclines in Bovine and Human Urine using a Graphite-Polyurethane Composite Electrode. *Anal. Lett.* **2015**, *48*, 1454–1464. [CrossRef]
56. Que, X.; Chen, X.; Fu, L.; Lai, W.; Zhuang, J.; Chen, G.; Tang, D. Platinum-catalyzed hydrogen evolution reaction for sensitive electrochemical immunoassay of tetracycline residues. *J. Electroanal. Chem.* **2013**, *704*, 111–117. [CrossRef]
57. Wangfuengkanagul, N.; Siangproh, W.; Chailapakul, O. A flow injection method for the analysis of tetracycline antibiotics in pharmaceutical formulations using electrochemical detection at anodized boron-doped diamond thin film electrode. *Talanta* **2004**, *64*, 1183–1188. [CrossRef]
58. Charoenraks, T.; Palaharn, S.; Grudpan, K.; Siangproh, W.; Chailapakul, O. Flow injection analysis of doxycycline or chlortetracycline in pharmaceutical formulations with pulsed amperometric detection. *Talanta* **2004**, *64*, 1247–1252. [CrossRef] [PubMed]
59. Treetepvijit, S.; Preechaworapun, A.; Praphairaksit, N.; Chuanuwatanakul, S.; Einaga, Y.; Chailapakul, O. Use of nickel implanted boron-doped diamond thin film electrode coupled to HPLC system for the determination of tetracyclines. *Talanta* **2006**, *68*, 1329–1335. [CrossRef] [PubMed]
60. Allahverdiyeva, S.; Yardım, Y.; Senturk, Z. Electrooxidation of tetracycline antibiotic demeclocycline at unmodified boron-doped diamond electrode and its enhancement determination in surfactant-containing media. *Talanta* **2021**, *223*, 121695. [CrossRef] [PubMed]
61. Loetanantawong, B.; Suracheep, C.; Somasundrum, M.; Surareungchai, W. Electrocatalytic Tetracycline Oxidation at a Mixed-Valent Ruthenium Oxide-Ruthenium Cyanide-Modified Glassy Carbon Electrode and Determination of Tetracyclines by Liquid Chromatography with Electrochemical Detection. *Anal. Chem.* **2004**, *76*, 2266–2272. [CrossRef] [PubMed]
62. Charoenraks, T.; Chuanuwatanakul, S.; Honda, K.; Yamaguchi, Y.; Chailapakul, O. Analysis of tetracycline antibiotics using HPLC with pulsed amperometric detection. *Anal. Sci.* **2005**, *21*, 241–245. [CrossRef] [PubMed]
63. Pizan-Aquino, C.; Wong, A.; Aviles-Felix, L.; Sotomayor, M.D.P.T. Evaluation of the performance of selective M-MIP to tetracycline using electrochemical and HPLC-UV method. *Mater. Chem. Phys.* **2020**, *245*, 122777. [CrossRef]
64. Ji, H.; Wang, E. Flow injection amperometric detection based on ion transfer across a water—Solidified nitrobenzene interface for the determination of tetracycline and terramycin. *Analyst* **1988**, *113*, 1541–1543. [CrossRef]
65. Agüí, L.; Guzman, A.; Pedrero, M.; Yáñez-Sedeño, P.; Pingarrón, J.M. Voltametric and flow injection determination of oxytetracycline residues in food samples using carbon fiber microelectrodes. *Electroanalysis* **2003**, *15*, 601–607. [CrossRef]
66. Oungpipat, W.; Southwell-Keely, P.; Alexander, P.W. Flow injection detection of tetracyclines by electrocatalytic oxidation at a nickel-modified glassy carbon electrode. *Analyst* **1995**, *120*, 1559–1565. [CrossRef]
67. Hou, W.; Wang, E. Liquid chromatographic determination of tetracycline antibiotics at an electrochemically pre-treated glassy carbon electrode. *Analyst* **1989**, *114*, 699–702. [CrossRef]
68. Felipe Montiel, N.; Parrilla, M.; Beltran, V.; Nuyts, G.; Van Durme, F.; De Wael, K. The opportunity of 6-monoacetylmorphine to selectively detect heroin at preanodized screen printed electrodes. *Talanta* **2021**, *226*, 122005. [CrossRef] [PubMed]
69. Schram, J.; Parrilla, M.; Sleegers, N.; Samyn, N.; Bijvoets, S.M.; Heerschop, M.W.J.; van Nuijs, A.L.N.; De Wael, K. Identifying electrochemical fingerprints of ketamine with voltammetry and LC-MS for its detection in seized samples Identifying electrochemical fingerprints of ketamine with voltammetry and LC-MS for its detection in seized samples. *Anal. Chem.* **2020**, *92*, 13485–13492. [CrossRef]
70. Van Echelpoel, R.; de Jong, M.; Daems, D.; Van Espen, P.; De Wael, K. Unlocking the full potential of voltammetric data analysis: A novel peak recognition approach for (bio)analytical applications. *Talanta* **2021**, *233*, 122605. [CrossRef]

71. Mirceski, V.; Skrzypek, S.; Stojanov, L. Square-wave voltammetry. *ChemTexts* **2018**, *4*, 1–14. [CrossRef]
72. Wang, H.; Zhao, H.; Quan, X. Gold modified microelectrode for direct tetracycline detection. *Front. Environ. Sci. Eng. China* **2012**, *6*, 313–319. [CrossRef]
73. Dang, X.; Hu, C.; Wei, Y.; Chen, W.; Hu, S. Sensitivity improvement of the oxidation of tetracycline at acetylene black electrode in the presence of sodium dodecyl sulfate. *Electroanalysis* **2004**, *16*, 1949–1955. [CrossRef]
74. Turku, I.; Sainio, T.; Paatero, E. Thermodynamics of tetracycline adsorption on silica. *Environ. Chem. Lett.* **2007**, *5*, 225–228. [CrossRef]
75. Ghadim, E.E.; Manouchehri, F.; Soleimani, G.; Hosseini, H.; Kimiagar, S.; Nafisi, S. Adsorption properties of tetracycline onto graphene oxide: Equilibrium, kinetic and thermodynamic studies. *PLoS ONE* **2013**, *8*, e79254. [CrossRef]
76. Schram, J.; Parrilla, M.; Sleegers, N.; Van Durme, F.; Van Den Berg, J.; van Nuijs, A.L.N.; De Wael, K. Electrochemical profiling and LC-MS characterization of synthetic cathinones: From methodology to detection in forensic samples. *Drug Test. Anal.* **2021**. [CrossRef]
77. Wu, J.; Zhang, H.; Oturan, N.; Wang, Y.; Chen, L.; Oturan, M.A. Application of response surface methodology to the removal of the antibiotic tetracycline by electrochemical process using carbon-felt cathode and DSA (Ti/RuO_2-IrO_2) anode. *Chemosphere* **2012**, *87*, 614–620. [CrossRef]
78. Wang, J.; Zhi, D.; Zhou, H.; He, X.; Zhang, D. Evaluating tetracycline degradation pathway and intermediate toxicity during the electrochemical oxidation over a Ti/Ti_4O_7 anode. *Water Res.* **2018**, *137*, 324–334. [CrossRef] [PubMed]
79. Forsberg, K.J.; Patel, S.; Wencewicz, T.A.; Dantas, G. The Tetracycline Destructases: A Novel Family of Tetracycline-Inactivating Enzymes. *Chem. Biol.* **2015**, *22*, 888–897. [CrossRef]
80. Volkers, G.; Petruschka, L.; Hinrichs, W. Recognition of drug degradation products by target proteins: Isotetracycline binding to tet repressor. *J. Med. Chem.* **2011**, *54*, 5108–5115. [CrossRef]